



Crosslinked norbornene copolymer anion exchange membrane for fuel cells

Chao Wang^{a,g,*}, Biming Mo^{c,1}, Zhenfeng He^{b,*}, Qian Shao^d, Duo Pan^{d,h}, Evan Wujick^f,
Jiang Guo^{i,*}, Xinling Xie^{e,h}, Xiaofeng Xie^g, Zhanhu Guo^{h,*}



^a College of Materials Science and Engineering, North University of China, Taiyuan 030051, China

^b National Demonstration Center for Experimental Chemical Engineering Comprehensive Education, School of Chemical Engineering and Technology, North University of China, Taiyuan 030051, China

^c School of Science, North University of China, Taiyuan 030051, China

^d College of Chemical and Environmental Engineering, Shandong University of Science and Technology, Qingdao 266590, China

^e School of Chemistry and Chemical Engineering, Guangxi Key Laboratory of Petrochemical Resource Processing and Process Intensification Technology, Guangxi University, Nanning 530004, China

^f Materials Engineering and Nanosensor [MEAN] Laboratory, Department of Chemical and Biological Engineering, The University of Alabama, Tuscaloosa, USA

^g INET, Tsinghua University, Beijing 100084, China

^h Integrated Composites Laboratory (ICL), Department of Chemical & Biomolecular Engineering, University of Tennessee, Knoxville, TN 37996, USA

ⁱ Engineered Multifunctional Composites (EMC) Nanotech. LLC., Knoxville, TN 37934, USA

ARTICLE INFO

Keywords:

Dynamic simulation
Anion exchange membrane
Norbornene
Ring-opening metathesis polymerization
Fuel cell

ABSTRACT

A series of crosslinked anion exchange membranes (AEMs) were prepared through ring-opening metathesis polymerization (ROMP) of tetraalkylammonium-functionalized norbornene derivatives. Dimensional stability and mechanical properties were enhanced by the crosslinker of 2, 2'-(hexane-1,6-diyl) bis(2-methyl-2, 3, 3a, 4, 7, 7a-hexahydro-1H-4, 7-methanoisindol-2-ium) iodide (b3). The thermal stability, ion exchange capacity (IEC), water uptake, swelling ratio, ion conductivity and mechanic property of the membranes were investigated. The molar ratios of monomer (3aR, 4S, 7R, 7aS)–2-methyl-2-(3-(trimethylammonio)propyl)–2, 3, 3a, 4, 7, 7a-hexahydro-1H-4,7-methanoisindol-2-ium iodide (a3): norbornene: monomer b3 was 1:6:3, 2:6:2, 3:6:1 in AEM-1, AEM-2, AEM-3. The resultant AEM-3 membrane had an IEC of 2.89 mmol g⁻¹, an ion conductivity of 64.79 mS cm⁻¹, a water absorption of 12.5% and a tensile strength of 15.18 MPa at 25 °C. The swelling ratio of AEM-1 (the molar ratio of monomer a3: norbornene: monomer b3 was 1:6:3) was 9.28% at 20 °C and 9.92% at 60 °C. The tensile strength of membranes was improved by the crosslinker. A single cell was built with this AEM-3 membrane and the performance was evaluated. A maximum power density of 152 mW cm⁻² at 50 °C was demonstrated. The membranes show great promise to serve as membranes for fuel cells due to excellent performances of higher ion conductivity and better dimensional stability.

1. Introduction

Anion exchange membranes (AEMs) have been applied to fuel cells for the advantages of low start-up temperature, good reliability and the possibility of using non-precious metals as catalysts [1–7]. As a core part of anion exchange membrane fuel cells (AEMFCs), anion exchange membranes (AEMs) transport hydroxide anions and prevent fuel from contacting with oxygen. The performance of AEMs directly affects stable operation of fuel cells, hence ideal AEMs should meet the following requirements: (1) low cost; (2) high ion conductivity; and (3) good mechanical and thermal stability properties [8].

Various kinds of AEMs had been prepared, such as quaternized high-performance commercial or synthesized polymers (polysulfone [9],

poly(2,6-dimethyl-1,4-phenylene oxide) (PPO) [10], poly-epichlorohydrin [11], poly(phenylene) backbone [12–15], polypyrrole backbone [16], poly(aryl ether oxadiazole) [17], etc) and radiation-grafted fluorinated polymers (poly(vinylidene fluoride), poly(ethylene-co-tetrafluoro ethylene) and poly(hexafluoropropylene-co-tetrafluoro ethylene)) [18]. In recent years, norbornene and its derivatives have been used for AEMs with their simple controllable polymerization technique, diverse sources of catalysts, easy modification and favorable thermal stability [19,20]. Ring-opening metathesis polymerization (ROMP) has been widely used for size-controlled polymerization. It has advantages of controlled segment structure and molecular size. Double bonds of circular olefin are opened and linked under the action of the catalyst [21,22]. However, common problems of low ion conductivity

* Corresponding authors.

E-mail addresses: wangchao_nuc@126.com (C. Wang), hezf@nuc.edu.cn (Z. He), jeremyjiangguo@gmail.com (J. Guo), xiexf@tsinghua.edu.cn (X. Xie), zguo10@utk.edu (Z. Guo).

¹ NOTE: Chao Wang and Biming Mo contributed equally to this work.

and poor stability restrict their wide application in industries [23]. Direct approaches to solve these problems are to increase the content of the functional groups (typically, quaternary ammonium) and cross-linking [24]. Recently, we have reported the synthesis of a new kind of tetraalkylammonium-functionalized linear AEMs with polynorbornene backbone [25,26]. Although the performance of the AEMs satisfies the working of fuel cell, but it is necessary to obtain excellent performances of AEM with a higher ion conductivity and better dimensional stability by optimizing the polynorbornene structure.

In present work, molecular modeling techniques were used to create amorphous cells composed of polymer molecules, hydroxide anions, and water molecules [27]. From the results of molecular dynamic (MD) simulation, the ionic diffusivity and coordination data between the polymer chain and ion were predicted. According to the computational data, the polymer molecular structure was designed and the polymer component was optimized. In order to improve dimensional stability, crosslinked copolymers were developed. The crosslinker not only offered benefits such as high thermal stability and enough strength but also provided functional groups. In this study, anion exchange membranes based on quaternary ammonium salt were prepared and their applications in H₂/O₂ fuel cell were evaluated with cell voltage and powered density.

2. Molecular modeling of structure and hydroxide anions diffusivity

2.1. Molecular modeling and simulation method

Molecular simulation has been applied to analyze the movement of ions and the microstructure of polymer backbone in membrane and to predict the chemical interactions between elements in the polymer and other mediums [28,29]. These computational modeling techniques have also been used to understand various membrane properties, including the ion transport behavior [30]. In this simulation, molecular simulations were conducted using the Material Studio software package (Accelrys Inc., USA). Amorphous cells with different quantities of water content were used to analyze ion diffusivity at different temperatures. Firstly, polymer chains, water molecules and hydroxide anions were constructed in Visualizer module. Model construction parameters are summarized in Table 1. Initial density of the cell was 1.0 g/cm³. Subsequently, smart algorithm was used for geometry optimization of the cell, and the global minimum configuration was found by simulated annealing. Furthermore, the cell reached equilibrium using the Forcite module with temperature and energy as the equilibrium criteria. In this step, NPT canonical ensemble was used for calculation. Time step was 1 fs and the total simulation time was set as 500 ps NPT at 300 and 330 K, respectively. All the molecular dynamics simulations were performed using the Ewald summation with the fine-accuracy of 0.001 kcal/mol. NHL thermostat and Andersen barostat were used to control the temperature and pressure during the simulations with a decay constant of 0.1 ps. After that, the density and energy of the cells kept constant, indicating that the system reached equilibrium. Then, mean square displacement (MSD) and radial distribution function (RDF) were calculated based on the molecules motion trails.

Table 1
Description of the simulated cells.

Cell	Degree of polymerization	Number of polymer chain	Number of quaternary ammoniums /chain	Number of hydroxide anions	Number of water molecules	Water content (wt%)	density (g/cm ³)	Volume (Å ³)
300 K	100	3	66	198	780	30	1.051	96,568.249
330 K	100	3	66	198	1300	50	1.053	111,219.815

2.2. Calculating equation

To study the interrelationship between particles and the distribution of particles in the polymer, the RDF analysis was used. The RDF could describe the structural characteristics accurately and provide the cluster status and coordination number. The RDF was calculated according to Eq. (1):

$$g_{A-B}(r) = \frac{V}{N_B} \cdot \frac{n_B}{4\pi r^2 dr} \quad (1)$$

where g_{A-B} is the occurrence probability of particle B around particle A, V is the total volume of the system, N_B is the number of particle B, n_B is the number of particle B at a distance of r from A.

In the simulation, the MSD was used for the movements of molecules. The analytical method of diffusion coefficient estimation and RDF was used. Particle diffusion in AEMs was heterogeneous, and the diffusion curves of OH⁻ and H₂O could be obtained with a change in time. The diffusion coefficient could be obtained from Eq. (2):

$$D = \frac{1}{6N} \lim_{t \rightarrow \infty} \frac{d}{dt} \sum_{j=1}^N [(r_j(t) - r_j(0))^2] = \frac{1}{6} \lim_{t \rightarrow \infty} \frac{dMSD(t)}{dt} \quad (2)$$

where D is diffusion coefficient, N is the number of diffusing particles, r is the distance, $r_j(t) - r_j(0)$ represents the displacement of a particle at time t from the initial position of the particle, and MSD is the mean square displacement.

2.3. Microstructure of simulated cells

Fig. 1 shows the polynorbornene chemical formula (a) and repeat units (b) which were used to build unit cell (c). The microstructure of the cell can be described as a hydrophobic polymer backbone penetrated by a network of three-dimensional interlinked hydrophilic channels of different diameters. The presence of channels containing mobile charge carriers was an important characteristic feature of solid state ionic conductors [31].

Fig. 2 shows the water distribution in cells. It was observed that the water channels at 330 K were more continuous than that at 300 K due to the fact that the volume of polymer backbone increased with increasing the temperature, causing the rise of water uptake. The water molecules filled in the three-dimensional polymer backbone, so the number of water molecules was increased with increasing the temperature.

To analyze the correlation of quaternary ammonium groups with hydroxide anions and water molecules, the RDF of N, H₂O and OH⁻ was calculated and shown in Fig. 3. The pair correlation function between water molecule and quaternary ammonium groups was revealed in Fig. 3(a). The first and largest peak occurred at 4.2 Å. The concentration of distribution of quaternary ammonium groups indicated that the functional groups were evenly distributed around water channels, forming the walls of water channels. Fig. 3(b) shows the pair correlation function between hydroxide anions and water molecules. It is clearly observed that the RDF has two peaks for both water contents. The first peak moved from 1.0 to 2.0 Å, and the second peak moved from 2.4 to 3.2 Å. It illustrated that the hydroxide anions were surrounded by two layers of water cluster due to hydrogen bond, meaning that the hydroxide anions were well solvated in the water phase. Fig. 3(c) presents that the electrostatic interaction holds a hydroxide anion around the quaternary ammonium at 4.8 and 5.5 Å for 30 and

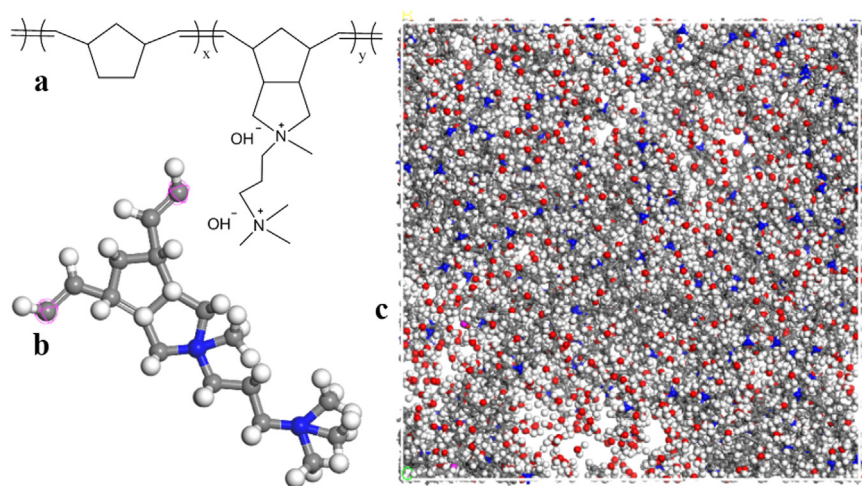


Fig. 1. The (a) polynorbornene chemical formula, (b) structure unit and (c) microstructure of unit cell with 50 wt% water uptake (red ball represents water).

50 wt% water uptake, respectively. The $g(r)$ of N-OH was weakened with increasing the water content through solvation. Hence, the correlation of quaternary ammonium groups with hydroxide decreased and hydroxide anions can spread out more broadly in the water channel.

2.4. Comparison of diffusion coefficient (D) and experimental work

In order to understand the diffusion behavior of the hydroxide anions in the polynorbornene membrane, the MSD of the hydroxide anions in the membranes was analyzed. Fig. 4 illustrates the slope of hydroxide anions for MSD of the polynorbornene membranes. The MSD of hydroxide anions with 50 wt% water content at 330 K was larger than that with 30 wt% water content at 330 K. It indicated that the hydroxide anions in the cell with 50 wt% water content at 300 K had a longer trajectory and a better mobility.

As the previous work reported that the simulated diffusion coefficients of water in the membranes exhibited the same trend as the experimental data [25,32]. The ion conductivity increased with increasing the temperature, in accordance with increasing water molecules and transport channel size inside the membrane. The kinetic energy of the molecules changed with increasing the temperature, the hydroxide anions had a larger kinetic energy at a higher temperature. Besides, water content and channel size could provide a platform on which hydroxide anions performed migration, combining with Grotthuss mechanisms [33] in the hydrated membranes and the *en mass* (vehicle) [34]. High water content contributed to the formation of

continuous water channels, which favored the transmission of hydroxide anions.

3. Experiments

3.1. Materials

Endic anhydride, lithium aluminium hydride, 1,6-Diaminohexane, 3-Dimethylaminopropylamine and magnesium sulfate were purchased from Aladdin. Acetic acid glacial, methanol, toluene, dichloromethane, and diethyl ether were obtained from Beijing Chemical Works. The Grubbs 3rd Generation catalyst was purchased from Energy Chemical and used as received. Deionized water was used and the resistance was 16Ω . All the chemical reagents used in the experiments were of reagent grade.

3.2. Preparation of membranes

The synthesis process of monomer (3aR,4S,7R,7aS)–2-methyl-2-(3-(trimethylammonio) propyl)–2,3,3a,4,7,7a-hexahydro-1H-4,7-methanoisindol-2-ium iodide (a3) and (3aR,7aS)–2-methyl-2-(6-((3aR,4S,7R,7aS)–2-methyl-2,3,3a,4,7,7a-hexahydro-1H-4,7-methanoisindol-2-ium-2-yl)hexyl)–2,3,3a,4,7,7a-hexahydro-1H-4,7-methanoisindol-2-ium iodide (b3) is shown in Figs. 5 and 6 [25,26], respectively. Crosslinked AEMs were prepared with monomer a3 and norbornene (NB), accompanied by monomer b3 as crosslinkers as shown in Fig. 7. As an example, the procedure used to prepare AEM-3

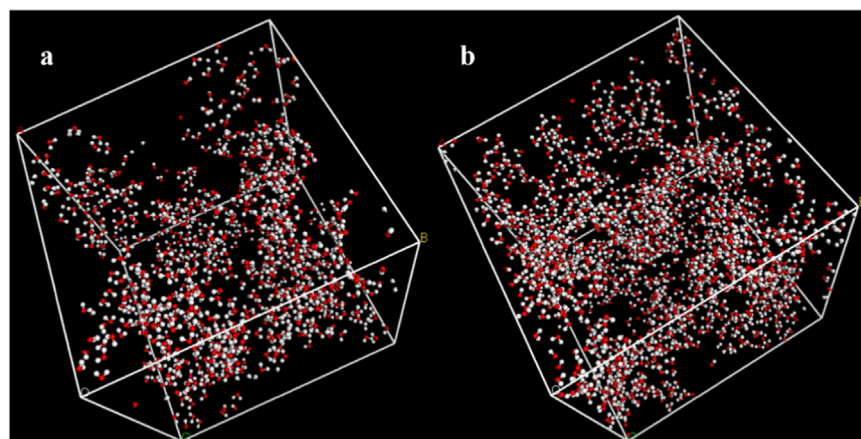


Fig. 2. Distribution of water molecules in the cell with a water uptake of (a) 30 wt% and (b) 50 wt%.

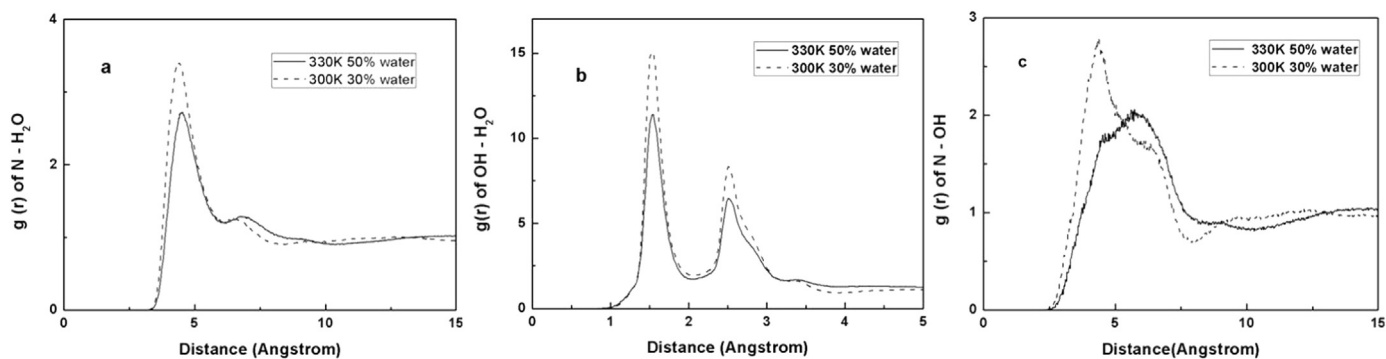


Fig. 3. Radial distribution functions of (a) N-H₂O, (b) OH-H₂O and (c) N-OH.

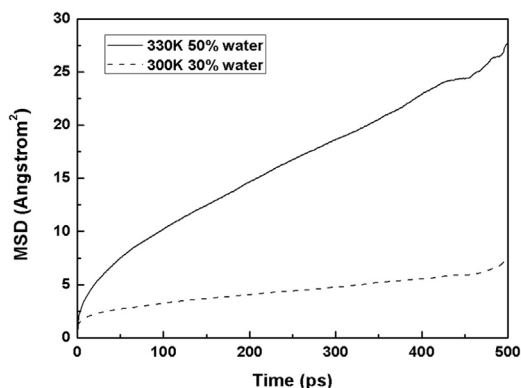


Fig. 4. Mean square displacement of hydroxide ions.

(which was subsequently identified to be the optimal formulation) was stated as follows: monomer a3 (81.4 mg, 0.325 mmol), norbornene (61.2 mg, 0.065 mmol), b3 (69 mg, 0.108 mmol) were dissolved in CH₂Cl₂ and CH₃OH (5 mL). Grubbs III catalyst (4.79 mg, 0.00542 mmol) was added. The resultant mixture was stirred for 30 min at 40 °C to obtain the casting solution. The solution was then cast onto a glass plate and dried at 25 °C until the solvent was removed. The membrane was peeled off from the glass plate under water to obtain the crosslinked AEM-3.

3.3. Ion exchange capacity (IEC)

The membrane IEC was measured by titration. To obtain the Cl⁻ counterion of the membrane, the AEMs were immersed in 0.5 M NaCl solution for 24 h and subsequently washed with deionized water several times. The Cl⁻ form of the AEMs was immersed in a fixed volume of 0.5 M NaNO₃ aqueous solution for 24 h. The amount of replaced chloride ions was titrated against 0.05 M AgNO₃ solution using K₂CrO₄ (10%) as an indicator. The IEC was calculated according to Eq. (3):

$$\text{IEC} = \frac{0.05 \text{ mol} \cdot \text{L}^{-1} \times V(\text{AgNO}_3)}{m_d} \quad (3)$$

where V_{AgNO₃} (mL) is the volume of the AgNO₃ solution, C_{AgNO₃} (mol·L⁻¹) is the concentration of AgNO₃ solution, and W_d (g) is the weight of the dried membrane sample.

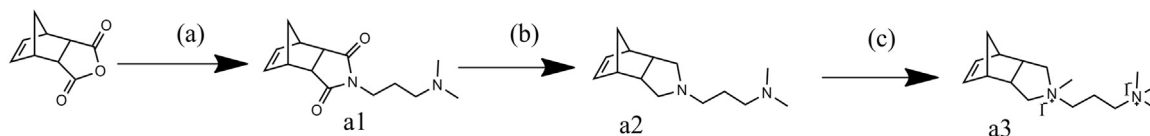


Fig. 5. Synthetic procedure for monomer a3 [25]: (a) C₇H₈, 80 °C, 24 h. (b) CH₂Cl₂, Et₂O, 0 °C, 24 h. (c) CH₃OH, 20 °C, 48 h.

3.4. Water uptake and swelling ratio

Water uptake and swelling ratio of AEMs were determined using the following procedures. The membrane was first dried under vacuum at 80 °C for 24 h, following which its weight and dimensions were accurately measured. Then the membrane was immersed into deionized water at a given temperature. After equilibration for 24 h, the membrane was recovered, and the surface water was blotted with a filter paper, the weight and dimensions were measured. The water uptake (W_u) and swelling ratio (S_r) were determined using Eqs. (4) and (5):

$$w_u = \frac{m_w - m_d}{m_d} \times 100\% \quad (4)$$

$$S_r = \frac{L_w - L_d}{L_d} \times 100\% \quad (5)$$

where m_w (g) and m_d (g) are the weight of the wet and dry membrane sample, respectively; L_d (cm) and L_w (cm²) respectively are the length of the membrane before and after water absorption.

3.5. Mechanical properties

The mechanical properties (stress-strain) of the crosslinked AEMs were studied at room temperature using a SHIMADZU AG-I 1 kN instrument at a strain rate of 5 mm/min. All the dumbbell thin films samples refer to National standard GB13022-1991. For each film, five replicates were tested.

3.6. Conductivities

According to impedance spectroscopy, the ionic conductivity (σ) of the membrane was obtained by using a Zahner IM6ex electrochemical workstation with an AC perturbation of 10 mV and over the frequency ranges from 100 MHz to 1 MHz. The membrane was immersed in deionized water for 24 h before testing. The membrane sample was clamped between four Pt electrodes using two Teflon® blocks, placed in deionized water at 25 °C, and evaluated. The conductivity of the membrane was calculated by Eq. (6):

$$\sigma = \frac{L}{RS} \quad (6)$$

where R (Ω) is the real impedance corresponding to zero phase angle in the impedance spectrum, L (cm) is the distance between two Pt electrodes, and S (cm²) is the cross-sectional area of the membrane

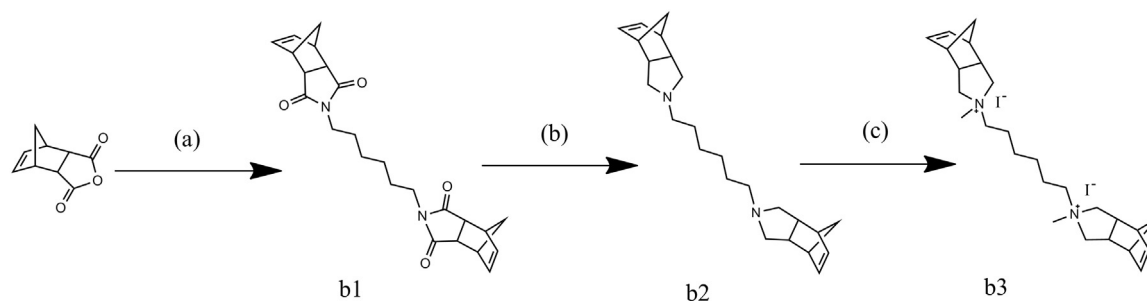


Fig. 6. Synthetic procedure for monomer b3 [26]: (a) CH_3COOH , 120°C , 6 h. (b) CH_2Cl_2 , Et_2O , 0°C , 24 h. (c) CH_3OH , 20°C , 48 h.

orthogonal to 1.

3.7. H_2/O_2 fuel cell

The MEA (Membrane of Electrode Assemblies) of AEM-3 membrane was made by spray casting solution on carbon paper (Pt/C 0.65 mg cm^{-2}) at 50°C , and assembling the anode, cathode and membrane without hot pressing into the fuel cells. The effective electrode area was 6.25 cm^2 . Hydrogen and oxygen under a pressure of 1.5/1 bar were pumped in two sides of a single cell with gas humidification.

4. Results and discussion

4.1. FTIR

Fig. 8 shows the FTIR spectra of a3, b3 and AEM-3. A broad absorption peak at 3449.25 cm^{-1} is due to the existence of quaternary ammonium groups [25]. The characteristic peaks between 2990 and 3060 cm^{-1} and 1640 cm^{-1} are the characteristic vibration of C-H and C=C bond respectively [26]. These observations confirmed the successful synthesis of polynorbornene.

4.2. TGA

The thermal degradation of the polymers studied by TGA showed that the cross-linked material was stable up to 240°C and only a few percent weight loss was observed due to the moisture evaporation in the material. As seen in Fig. 9, three stages were observed in the decomposition process. The initial decomposition temperature was about 240°C , the polymer showed about 30% weight loss between 240 and 300°C due to the decomposition of quaternary ammonium groups [27]. The temperature for side chains decomposition was at about 325°C , the polymer backbone shows good heat-resistance, with a decomposing temperature of 476°C . The results indicated that polynorbornene had an excellent thermal stability below 240°C , which was high enough to

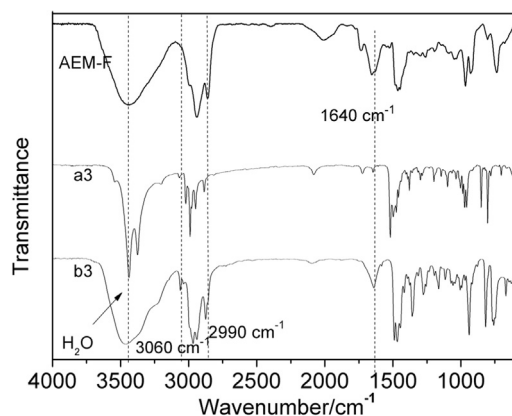


Fig. 8. FT-IR spectra of a3, b3 and AEM-3.

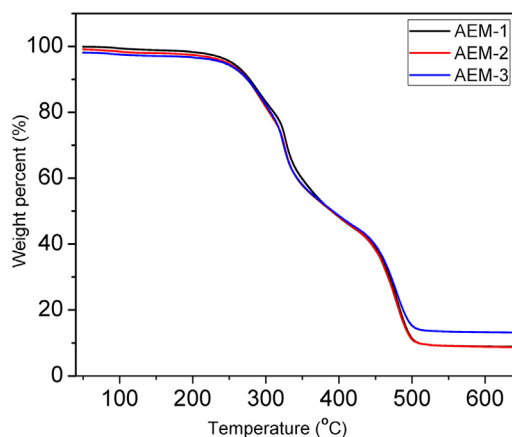


Fig. 9. TG curves for different polymers under N_2 atmosphere.

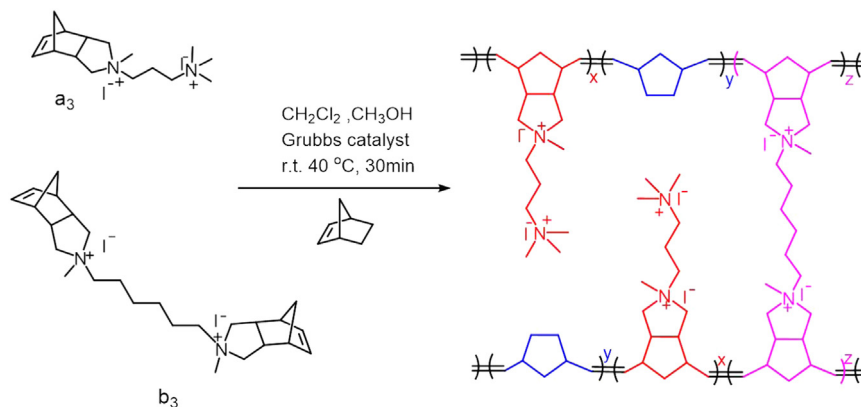


Fig. 7. Procedure for AEMs synthesis.

Table 2
IEC, water uptake and swelling ratio of the AEMs.

Measurement	AEM-1	AEM-2	AEM-3
IEC ($\text{mmol}\cdot\text{g}^{-1}$)	2.46 ± 0.04	2.72 ± 0.03	2.89 ± 0.05
Water uptake $_{t25}$ (%)	13.25 ± 2.15	15.23 ± 2.18	31.52 ± 2.86
Water uptake $_{t60}$ (%)	16.59 ± 2.35	18.91 ± 1.92	42.76 ± 2.13
Swelling ratio $_{t25}$ (%)	9.28 ± 1.60	10.25 ± 2.07	12.45 ± 1.97
Swelling ratio $_{t60}$ (%)	9.92 ± 1.30	12.34 ± 2.49	18.32 ± 2.18

Note : \pm Std. Dev means the mean-variance.

meet the using conditions of AEMFCs.

4.3. IEC, water uptake and swelling ratio

In order to improve the ionic conductivity, a series of cross-linked AEMs were prepared. The use of crosslinker can enhance the dimensional stability and mechanical properties [35]. Crosslinking density were increased with increasing the catalyst loading while the ion conductivity was reduced [36,37]. Herein, all membranes had a [olefin]: [catalyst] loading of 200:1. The IEC increased from 2.46 to 2.89 mmol g^{-1} with increasing a3 content (from AEM-1 to AEM-3). The IEC has a high impact on the ionic conductivity and water uptake. While excessive water uptake results in an unacceptable dimensional instability and a lower conductivity due to the gel formation and reduction in the ionic mobility. Detailed characterization data of AEMs are listed in Table 2.

Water uptake and swelling ratio for anion exchange membrane were measured at 25 and 60 °C. It has been known that adequate water uptake is needed to form interconnected hydrated channel, ensuring maximal ionic conductivity [38,39]; however, excessive water uptake may also lead to a detrimental loss of mechanical integrity and decreased ion conductivity [40,41]. Meanwhile, an ideal membrane will not swell appreciably in length, width, or thickness upon exposure to solvents contained within a fuel cell at typical operating temperatures [24]. As we can see from Table 2, water uptake and swelling ratio increased quickly with IEC changed from 2.46 to 2.89 mmol g^{-1} . The performance of the prepared films was acceptable. The swelling ratio of AEM-1 was 9.28% at 25 °C and 9.92% at 60 °C, and the performance of the prepared films of AEM-3 was better than AEM-1.

4.4. Mechanical properties

Fig. 10 shows the mechanical properties of the crosslinked membranes. The crosslinked membranes showed a significantly improved tensile strength as compared to the linear membranes, which had a tensile strength of 6.19 MPa. As for AEM-3, high crosslinking ratio restricted the swelling ratio to 18.32%. Crosslinking increased the tensile strength and had a tensile strength of 14.64, 12.81 and 15.18 MPa,

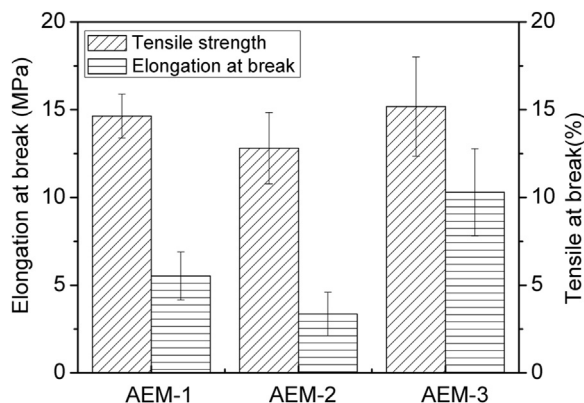


Fig. 10. The mechanical properties of the crosslinked membranes.

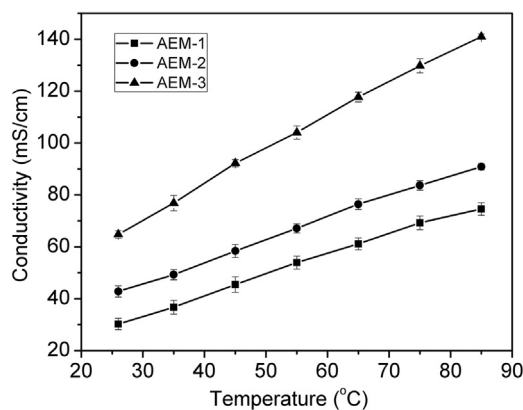


Fig. 11. Hydroxide ion conductivity of anion exchange membranes.

respectively. Crosslinker increased the tensile strength, which was meaningful to maintain the membrane stability. These results indicated that all the membranes were stronger than the linear polymer membrane [25] and tough enough for potential use as AEMs.

4.5. Hydroxide ion conductivities

Fig. 11 shows the hydroxide ion conductivity of AEMs. A positive correlation between the conductivity and temperature can be observed. All AEMs membranes exhibited a room temperature ion conductivity higher than $30 \text{ mS}\cdot\text{cm}^{-1}$. In the deionized water, AEM-1, AEM-2 and AEM-3 membranes exhibited an ion conductivity of 30.22, 42.81 and $64.79 \text{ mS}\cdot\text{cm}^{-1}$ at 25 °C, respectively. As the temperature increases, the free volume becomes inflated, and the anion transferring channels become wider, causing a strengthening of the overall mobility of ions and polymer chains. It was noteworthy that the conductivity of AEM-3 membrane was much higher than that of the AEM-1 and AEM-2, probably due to the decrease of distance between the functional ammonium groups with increasing the a3 content [42].

4.6. Single fuel cell performance

MEA of AEM-3 membrane was made by spray casting solution and catalyst on the carbon paper (Pt/C 0.65 mg cm^{-2}) at 50 °C, assembling anode, cathode and membrane without hot pressing into fuel cell. The effective electrode area was 6.25 cm^2 . Hydrogen and oxygen under a pressure of 1.5/1 bar were pumped into the single cell with gas humidification. Fig. 12 shows the polarization curve of a single cell at 50 °C with a 70% relative humidity. It can be noted that the open circuit voltage is approximately 1.03 V, this means that the fabricated membrane can block fuel finely. When the current density is 350 mA cm^{-2} ,

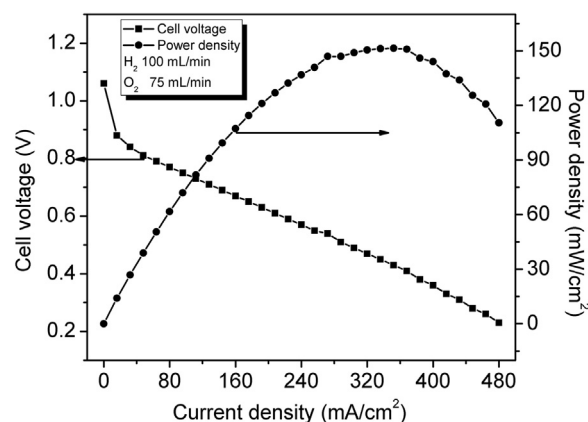


Fig. 12. Fuel cell performance based on AEM-3 at 50 °C.

the fuel cell shows a maximum power density of more than 152 mW cm^{-2} . The good performance can be attributed to the high ion conductivity of AEM-3.

5. Conclusion

In summary, a series of crosslinked polynorbornene were prepared. The anion exchange membranes were obtained with a solution casting method and followed by hydroxide exchanging in a sodium hydroxide solution. With increasing the amount of a3, the IEC, water uptake, mechanical properties, and ion conductivity of AEM were highly increased. Crosslinking not only restricted the swelling ratio of membranes, but also increased the dimensional stability. The AEM-3 membranes had an high ion conductivity of 64.79 mS cm^{-1} at 25°C . Moreover, AEM-3 had a tensile strength of 15.18 MPa . The IEC of all membranes was in the range from 2.46 to 2.89 mmol g^{-1} . The water uptake and swelling ratio of the AEMs varied from 16.59% to 42.67% and 9.92 – 18.32% at 60°C , respectively. According to the simulation results, high water content contributed to the formation of continuous water channels, which favored the transmission of hydroxide ions. All membranes owned a comprehensive property of dimensional and thermal stability. The H_2/O_2 single fuel cells testing using the AEM-3 membranes showed an open circuit voltage of 1.03 V and a maximum power density up to 152 mW cm^{-2} at 50°C . All the results suggested that the AEMs systems are promising for applications in fuel cells.

Acknowledgments

The work is funded by the National Natural Science Foundation of China (Project No. 51503187, 21504037, and 51603194); the National key R&D Project (Project No. 2016YFE0102700); the Shanxi provincial foundation for science and technology research (Project No. 201601D021058, 201701D221050). Partial support is also from the NIMHD-RCMI grant number 5G12MD007595 from the National Institute of Minority Health, Health Disparities and the NIGMS-BUILD grant number 8UL1GM118967 and National Science Foundation (Grant 1700429).

References

- [1] T.N. Danks, R.C.T. Slade, J.R. Varcoe, Alkaline anion-exchange radiation-grafted membranes for possible electrochemical application in fuel cells, *J. Mater. Chem.* 13 (2003) 712–721.
- [2] J. Fang, P.K. Shen, Quaternized poly(phthalazinone ether sulfone ketone) membrane for anion exchange membrane fuel cells, *J. Membr. Sci.* 285 (2006) 317–322.
- [3] L. Li, Y. Wang, Quaternized polyethersulfone Cardo anion exchange membranes for direct methanol alkaline fuel cells, *J. Membr. Sci.* 262 (2005) 1–4.
- [4] G. Merle, M. Wessling, K. Nijmeijer, Anion exchange membranes for alkaline fuel cells: a review, *J. Membr. Sci.* 377 (2011) 1–35.
- [5] Y. Wang, B. Peppley, K.A.M. Creber, V.T. Bui, E. Halliop, Preliminary evaluation of an alkaline chitosan-based membrane fuel cell, *J. Power Sources* 162 (2006) 105–113.
- [6] (a) Y. Li, B. Zhou, G. Zheng, X. Liu, et al., Continuously prepared highly conductive and stretchable SWNTs/MWNTs synergistically composited electrospun thermoplastic polyurethane yarns for wearable sensing, *J. Mater. Chem. C* 6 (2018) 2258–2269; (b) H. Du, et al., C. Zhao, J. Lin, Z. Hu., Carbon nanomaterials in direct liquid fuel cells, *Chem. Record* (2018), <http://dx.doi.org/10.1002/ctr.201800008> in press; (c) Q. Jiang, L. Wang, C. Yan, C. Liu, Z. Guo, N. Wang, *Eng. Sci.* (2018), <http://dx.doi.org/10.30919/es.180329> in press.
- [7] (a) W. Deng, T. Kang, H. Liu, J. Zhang, N. Wang, N. Lu, Y. Ma, A. Umar, Z. Guo, Potassium hydroxide activated and nitrogen doped graphene with enhanced supercapacitive behavior, *Sci. Adv. Mater.* (2018), <http://dx.doi.org/10.1166/sam.2018.3279> in press; (b) F. Ran, X. Yang, L. Shao, Recent progress in carbon-based nanoarchitectures for advanced supercapacitors, *Adv. Compos. Hybrid Mater.* 1 (2018) 32–55; (c) L. Yan, H. Wang, D. Huang, H. Luo, Electrodes with high conductivities for high performance lithium/sodium ion batteries, *Eng. Sci.* (2018), <http://dx.doi.org/10.30919/es.180318> in press; (d) X. Wang, X. Zeng, D. Cao, Biomass-derived nitrogen-doped porous carbons (NPC) and NPC/polyaniline composites as high performance supercapacitor materials, *Eng. Sci.* (2018), <http://dx.doi.org/10.30919/es.180325> in press.
- [8] T.S. Olson, S. Pilypenko, P. Atanassov, K. Asazawa, K. Yamada, H. Tanaka, Anion exchange membrane fuel cells dual-site mechanism of oxygen reduction reaction in alkaline media on cobaltpolypyrrole electrocatalysts, *J. Phys. Chem. C* 144 (2010) 5049–5559.
- [9] S. Gu, R. Cai, T. Luo, K. Jensen, C. Contreras, Y. Yan, Quaternary phosphonium-based polymers as hydroxide exchange membranes, *ChemSusChem* 3 (2010) 555–558.
- [10] L. Wu, T. Xu, Improving anion exchange membranes for DMAFCs by inter-cross-linking CPPO/BPPO blends, *J. Membr. Sci.* 322 (2008) 286–292.
- [11] D. Stoica, L. Ogiev, L. Akrou, F. Alloin, J.F. Fauvarque, Anionic membrane based on polyepichlorhydrin matrix for alkaline fuel cell: synthesis, physical and electrochemical properties, *Electrochim. Acta* 53 (2007) 1596–1603.
- [12] M.R. Hibbs, C.H. Fujimoto, C.J. Cornelius, Synthesis and characterization of poly(phenylene)-based anion exchange membranes for alkaline fuel cells, *Macromolecules* 42 (2009) 8316–8321.
- [13] L. Liu, X. Chu, J. Liao, Y. Huang, Yi. Li, Z. Ge, M.A. Hickner, N. Li, Tuning the properties of poly(2,6-dimethyl-1,4-phenylene oxide) anion exchange membranes and their performance in H_2/O_2 fuel cells, *Energy Environ. Sci.* 11 (2018) 435–446.
- [14] Z. Liu, et al., Mechanical enhancement of melt-stretched β -nucleated isotactic polypropylene: the role of lamellar branching of β -crystal, *Polym. Test.* 58 (2017) 227–235.
- [15] J. Jiang, X. Liu, M. Lian, Y. Pan, et al., Self-reinforcing and toughening isotactic polypropylene via melt sequential injection molding, *Polym. Test.* 67 (2018) 183–189.
- [16] X. Cheng, S. Ding, J. Guo, C. Zhang, Z. Guo, L. Shao, In-situ interfacial formation of TiO_2 /polypyrrole selective layer for improving the separation efficiency towards molecular separation, *J. Membr. Sci.* 536 (2017) 19–27.
- [17] G. Liu, Y. Shang, X. Xie, S. Wang, J. Wang, Y. Wang, Synthesis and characterization of anion exchange membranes for alkaline direct methanol fuel cells, *Int. J. Hydrog. Energy* 37 (2012) 848–853.
- [18] J. Fang, Y. Yang, X. Lu, M. Ye, W. Li, Y. Zhang, Cross-linked, ETFE-derived and radiation grafted membranes for anion exchange membrane fuel cell applications, *Int. J. Hydrog. Energy* 37 (2012) 594–602.
- [19] Y. Zha, M.L. Disabb-Miller, Z.D. Johnson, M.A. Hickner, G.N. Tew, Metal-cation-based anion exchange membranes, *J. Am. Chem. Soc.* 134 (2012) 4493–4496.
- [20] Y. Zhao, X. Li, Z. Feng, X. Xie, C. Chai, Y. Luo, Progress of ion exchange membrane based on poly(norbornene)s derivatives via ring-opening metathesis polymerization, *J. Chem. Ind. Eng. (China)* 66 (2015) 10–16.
- [21] T.J. Clark, N.J. Robertson, H.A. Kostalik IV, E.B. Lobkovsky, P.F. Mutolo, H.D. Abruña, A ring opening metathesis polymerization route to alkaline anion exchange membranes development of hydroxide conducting thin films from an ammonium functionalized monomer, *J. Am. Chem. Soc.* 131 (2009) 12888–12889.
- [22] N.J. Robertson, H.A. Kostalik IV, T.J. Clark, P.F. Mutolo, H.D.A. Bruña, G.W. Coates, Tunable high performance cross-linked alkaline anion exchange membranes for fuel cell applications, *J. Am. Chem. Soc.* 132 (2010) 3400–3440.
- [23] S.Y. Shen, T.S. Zhao, J.B. Xu, Y.S. Li, Synthesis of PdNi catalysts for the oxidation of ethanol in alkaline direct ethanol fuel cells, *J. Power Sources* 195 (2010) 1001–1006.
- [24] W. Wang, S. Wang, W. Li, X. Xie, Y. Lv, Synthesis and characterization of a fluorinated cross-linked anion exchange membrane, *Int. J. Hydrog. Energy* 38 (2013) 11045–11052.
- [25] L. Feng, Y. Zhao, X. Xie, Preparation of tunable quaternary ammonium functionalized norbornene derivatives anion exchange membrane, *J. Chem. Ind. Eng. (China)* 66 (2015) 257–262.
- [26] Y. Zhao, L. Feng, J. Gao, Y. Zhao, S. Wang, V. Ramani, Study on tunable crosslinking anion exchange membranes fabrication and degradation mechanism, *Int. J. Hydrog. Energy* 41 (2016) 16264–16274.
- [27] C. Wang, Z. He, X. Xie, X. Mai, Y. Li, T. Li, M. Zhao, C. Yan, H. Liu, E.K. Wujcik, Z. Guo, Controllable crosslinking anion exchange membranes with excellent mechanical and thermal properties, *Macromol. Mater. Eng.* (2018), <http://dx.doi.org/10.1002/mame.201700462> in press.
- [28] X. Li, Y. Zhao, S. Wang, X. Xie, Molecular dynamics simulation study of a polynorbornene-based polymer: a prediction of proton exchange membrane design and performance, *Int. J. Hydrog. Energy* 41 (2016) 16254–16263.
- [29] Y. Zhao, X. Li, S. Wang, W. Li, X. Zhang, X. Xie, The Activity of Benzyl and Allyl α -H Sites in p-Cresol-grafted Fluorinated Poly(aryl ether oxadiazole) toward the Bromination Reaction, *Chem. Lett.* 43 (2014) 1943–1945.
- [30] D.J. Kim, C.H. Park, S.Y. Nam, Molecular dynamics simulations of modified PEEK polymeric membrane for fuel cell application, *Int. J. Hydrog. Energy* (41) (2016) 7641–7648.
- [31] B.V. Merinov, W.A. Goddard, Computational modeling of structure and OH-anion diffusion in quaternary ammonium polysulfone hydroxide-Polymer electrolyte for application in electrochemical devices, *J. Membr. Sci.* 431 (2013) 79–85.
- [32] C. Wang, B. Mo, Z. He, X. Xie, C. Zhao, L. Zhang, Q. Shao, X. Guo, E.K. Wujcik, Z. Guo, Hydroxide ions transportation in polynorbornene anion exchange membrane, *Polymer* 138 (2018) 363–368.
- [33] K.N. Grew, W.K.S. Chiu, A dusty fluid model for predicting hydroxyl anion conductivity in alkaline anion exchange membranes, *J. Electrochem. Soc.* 157 (2010) 327–337.
- [34] K.D. Kreuer, A. Rabenau, W. Weppner, A new model for the interpretation of the conductivity of fast proton conductors, *Angew. Chem. Int. Ed.* 21 (1982) 208–209.
- [35] B. Bauer, H. Strathmann, F. Effenberger, Anion-exchange membranes with improved alkaline stability, *Desalination* 79 (1990) 125–144.
- [36] M.-H. Jeong, K.-S. Lee, J.-S. Lee, Cross-linking density effect of fluorinated aromatic polyethers on transport properties, *Macromolecules* 42 (2009) 1652–1658.
- [37] Y. Xiong, J. Fang, Q.H. Zeng, Q.L. Liu, Preparation and characterization of cross-linked quaternized poly(vinyl alcohol) membranes for anion exchange membrane

- fuel cells, *J. Membr. Sci.* 311 (2008) 319–325.
- [38] E.A. Weibera, D. Meisa, P. Jannasch, Anion conducting multiblock poly(arylene ether sulfone)s containing hydrophilic segments densely functionalized with quaternary ammonium groups, *Polym. Chem.* 6 (2015) 1986–1996.
- [39] Q. Li, L. Liu, Q. Miao, B. Jin, R. Bai, Hydroxide-conducting polymer electrolyte membranes from aromatic ABA triblock copolymers, *Polym. Chem.* 5 (2014) 2208–2213.
- [40] M.R. Hibbs, M.A. Hickner, T.M. Alam, S.K. McIntyre, C.H. Fujimoto, C.J. Cornelius, Transport properties of hydroxide and proton conducting membranes, *Chem. Mater.* 20 (2008) 2566–2573.
- [41] H.L.S. Salerno, F.L. Beyer, Y.A. Elabd, Anion exchange membranes derived from nafion precursor for the alkaline fuel cell, *J. Polym. Sci. Part B: Polym. Phys.* 50 (2012) 552–562.
- [42] J. Wang, H. Wei, S. Yang, H. Fang, P. Xu, Y. Ding, Constructing pendent imidazolium-based poly(phenylene oxide)s for anion exchange membranes using a click reaction, *RSC Adv.* 5 (2015) 93415–93422.